3D correlative electron microscopy reveals continuity of Brucellacontaining vacuoles with the endoplasmic reticulum

Sedzicki, Jaroslaw; Tschon, Therese; Low, Shyan Huey; Willemart, Kevin; Goldie, Kenneth N; Letesson, Jean-Jacques; Stahlberg, Henning; Dehio, Christoph

Published in:
Journal of Cell Science

DOI:
10.1242/jcs.210799

Publication date:
2018

Document Version
Publisher's PDF, also known as Version of record

© 2018. Published by The Company of Biologists Ltd | Journal of Cell Science (2018) 131, jcs210799. doi:10.1242/jcs.210799

RESEARCH ARTICLE

3D correlative electron microscopy reveals continuity of *Brucella*-containing vacuoles with the endoplasmic reticulum

Jaroslaw Sedzicki[1,2], Therese Tschon[1], Shyan Huey Low[1,*], Kevin Willemart[3], Kenneth N. Goldie[2], Jean-Jacques Letesson[3], Henning Stahlberg[2] and Christoph Dehio[1,‡]

ABSTRACT

Entry of the facultative intracellular pathogen *Brucella* into host cells results in the formation of endosomal *Brucella*-containing vacuoles (eBCVs) that initially traffic along the endocytic pathway. eBCV acidification triggers the expression of a type IV secretion system that translocates bacterial effector proteins into host cells. This interferes with lysosomal fusion of eBCVs and supports their maturation to replicative *Brucella*-containing vacuoles (rBCVs). Bacteria replicate in rBCVs to large numbers, eventually occupying most of the cytoplasmic volume. As rBCV membranes tightly wrap each individual bacterium, they are constantly being expanded and remodeled during exponential bacterial growth. rBCVs are known to carry endoplasmic reticulum (ER) markers; however, the relationship of the vacuole to the genuine ER has remained elusive. Here, we have reconstructed the 3-dimensional ultrastructure of rBCVs and associated ER by correlative structured illumination microscopy (SIM) and focused ion beam/scanning electron microscopic tomography (FIB/SEM). Studying *B. abortus*-infected HeLa cells and trophoblasts derived from *B. melitensis*-infected mice, we demonstrate that rBCVs are complex and interconnected compartments that are continuous with neighboring ER cisternae, thus supporting a model that rBCVs are extensions of genuine ER.

KEY WORDS: Endoplasmic reticulum, Replicative *Brucella*-containing vacuole, rBCV, FIB/SEM tomography, Correlative light and electron microscopy, CLEM, Sec61

INTRODUCTION

Several bacterial pathogens have adapted to an intracellular lifestyle. Eukaryotic host cells provide an environment for replication and persistence that is rich in nutrients and that shields the pathogens from different hostile factors, such as immunity mechanisms or competition with other microbes. An intracellular lifestyle has, however, many challenges of its own. Bacteria internalization by either phagocytic or non-phagocytic cells generates a vacuole equipped with various bactericidal mechanisms. Intracellular bacteria have developed various strategies that allow them to avoid these defenses and create conditions for their successful replication (Creasey and Isberg, 2014). The establishment and maintenance of an intracellular replicative niche suitable for efficient growth is a key feature of pathogens that decisively contributes to both their survival in the host and success in transmission to new hosts. Many bacteria have been shown to thrive inside specialized vacuoles that display at least some characteristics of host organelles. The nature of these compartments varies greatly depending on the pathogen. In some cases, growth occurs inside arrested early endosomes, *Mycobacterium tuberculosis* is one example (Fratti et al., 2003; Vergne et al., 2004). *Coxiella* forms a compartment characterized by the presence of autophagy markers (Gutierrez et al., 2005), while *Chlamydia* thrives in a modified vacuole derived from Golgi membranes (Delevoye et al., 2008). Finally, pathogens such as *Legionella* and *Brucella* replicate inside vacuoles that display characteristics of the endoplasmic reticulum (ER) (Celli and Tsolis, 2015).

Bacteria from the genus *Brucella* are facultative intracellular pathogens. They are the causative agents of brucellosis, a worldwide zoonosis that has serious health and economic impact. In the animal host, the bacteria target the reproductive organs, causing spontaneous miscarriage or weakening of offspring. Both lead to major losses in the livestock industry. The pathogen is transmitted from animals to humans mostly through contaminated dairy products. During chronic infection the bacteria get disseminated across different organs and cell types, including macrophages, dendritic cells and placental trophoblasts. This results in a progressive debilitating disease that is difficult to diagnose and treat, often leading to persistence and relapses (Archambaud et al., 2010; Atluri et al., 2011; Pappas et al., 2005).

Following internalization by host cells by a poorly described mechanism, bacteria are enclosed in a membranous compartment called the *Brucella*-containing vacuole (BCV), which initially displays endosome characteristics (eBCV). It acquires early endosome markers, such as Rab5 (mammals have Rab5a, Rab5b and Rab5c isoforms) and EEA1, followed by the emergence of late endosome markers such as LAMP1 and Rab7 (Rab7a and Rab7b) later in the maturation process (Bellaire et al., 2005; Celli et al., 2003; Comerci et al., 2001; Pizarro-Cerda et al., 1998a,b). The gradual acidification of the compartment triggers the expression of the VirB type IV secretion system (T4SS), which enables the translocation of a repertoire of effector proteins into the host cell cytoplasm (Boschiroli et al., 2002; Myeni et al., 2013; Porte et al., 1999). This prevents fusion of the eBCV with lysosomes and eventually leads to the formation of a replicative niche (replicative BCV or rBCV) that has certain characteristics of the ER (Comerci et al., 2001; Lestrate et al., 2000). This process is thought to occur through interactions of rBCVs with ER exit sites, but the details remain elusive (Celli et al., 2003; Pizarro-Cerda et al., 1998a,b; Taguchi et al., 2015). Once the replicative niche is established, *Brucella* undergoes numerous rounds of division until most

[1]Focal Area Infection Biology, Biozentrum, University of Basel, 4056 Basel, Switzerland. [2]Center for Cellular Imaging and NanoAnalytics (C-CINA), Biozentrum, University of Basel, 4056 Basel, Switzerland. [3]Microorganisms Biology Research Unit (URBM, Unité de Recherche en Biologie des Microorganismes), University of Namur, 5000 Namur, Belgium.
*Present address: Lee Kong Chian School of Medicine, Nanyang Technological University (NTU), Singapore 639798, Singapore.

‡Author for correspondence (christoph.dehio@unibas.ch)

S.H.L., 0000-0003-3512-433X; C.D., 0000-0001-7288-1052

Received 13 September 2017; Accepted 4 January 2018

Journal of Cell Science (2018) 131, jcs210799. doi:10.1242/jcs.210799

cytoplasmic volume of the host cell is occupied by bacteria, each tightly wrapped by rBCV membranes. It has been suggested that the intracellular life cycle is completed by the formation of autophagic BCVs (aBCVs), a process that may represent non-canonical action of autophagy initiation factors (Starr et al., 2012).

Despite numerous contributions regarding the nature and characteristics of the replicative niche of *Brucella*, many questions remain open. Not only do we lack knowledge of how the rBCV is established, but also a detailed description of its structure in relation to ER and other cellular organelles. The rBCV, which is often described as 'ER-derived' or 'ER-associated', has many interesting features (Case et al., 2016; Celli and Tsolis, 2015). It is widely accepted that its membrane is characterized by the presence of different ER markers, such as calnexin, calreticulin, Sec61β and associated ribosomes (Celli et al., 2003; Pizarro-Cerda et al., 1998a). Dividing bacteria have been shown to sit in individual, single-membrane compartments that are limited in space (Celli et al., 2003; Detilleux et al., 1990a; Pizarro-Cerda et al., 1998a,b). There have been several reports indicating fusion between rBCVs and the ER, and the presence of the bacteria in the perinuclear space (Anderson et al., 1986; Celli et al., 2003; Detilleux et al., 1990b), which suggests at least partial continuity between rBCVs and the ER network. The conclusions drawn in these examples are typically based on transmission electron microscopy (TEM) micrographs of ultrathin sections, which provide useful two-dimensional (2D) information on the nature of the rBCV, but do not reflect the complex three-dimensional (3D) structure of the ER (Nixon-Abell et al., 2016).

Here, we employed correlative structured illumination microscopy (SIM) (Gustafsson et al., 2008) and focused ion beam scanning electron microscopy (FIB/SEM) (Knott et al., 2011) to study the ultrastructural details of rBCVs and their relationship to the ER. FIB/SEM allows 3D imaging of biological samples at intermediate electron microscopy resolutions and has proved useful for the detailed description of subcellular structures. In combination with high-resolution light microscopy, this technique can resolve ultrastructure details of the interactions between organelles inside eukaryotic cells (Alcantara et al., 2017; Mellouk et al., 2014). Our unprecedented 3D reconstructions of membrane compartments in *Brucella*-infected cells allow the visualization of a network of luminal connections between rBCVs and the ER, supporting the hypothesis that the rBCV is an integral part of this organelle.

RESULTS

3D-CLEM reveals the 3D ultrastructure of the rBCV

In order to resolve the 3D ultrastructure of rBCVs in relation to other cellular organelles by a correlative light and electron microscopy (CLEM) approach, we used HeLa cells infected with *B. abortus* as a simple infection model. HeLa cells have been extensively used to study *Brucella* interaction with eukaryotic cells, and are easy to manipulate and relatively flat, which makes them well suited for microscopy. In order to specifically label ER membranes, we used HeLa cells expressing the ER markers calnexin–GFP (Lakkaraju et al., 2012) and Emerald–Sec61β (Nixon-Abell et al., 2016), both of which have previously been shown to colocalize with the rBCV (Pizarro-Cerda et al., 1998a).

SIM of HeLa cells infected with *B. abortus* for 24 h (or 48 h in the case of Fig. S1) indicated that the majority of the bacteria were residing, individually, inside compartments that stained positively for the ER markers (Fig. 1A; Fig. S1A). FIB/SEM tomography images of the corresponding cells revealed the arrangement of membranous organelles enclosing the bacteria. In HeLa cells expressing calnexin–GFP, we discovered the presence of multi-layered membrane artifacts that often formed around the BCVs (Fig. S1B). These structures probably represent previously reported multilayered ER assemblies induced by calnexin–GFP overexpression (Okiyoneda et al., 2004). While the data indirectly support the idea that the pathogen resides in the ER lumen, the artifactual changes of ER morphology preclude the use of this marker for detailed characterization of the rBCV.

FIB/SEM tomograms of cells expressing Emerald–Sec61β indicated that bacteria reside within single-membrane vacuoles (Fig. 1). The rBCVs were distributed across a large volume of the host cell cytoplasm, with different organelles interspersed between them. Most rBCVs apparently contained a single bacterium, which has been described as a characteristic trait of pathogens belonging to the genus *Brucella* (Case et al., 2016). Some of the bacteria visualized were undergoing division (Fig. 1A,B). Occasionally, more than one bacterium was present inside the same rBCV (Fig. 1B). Our EM data indicate that rBCV membranes are tightly associated with the surface of the bacteria. During bacterial division, when the daughter cells become separated, rBCV membranes were found to tighten around the invaginations of the central septum, keeping the volume of the rBCV lumen to the minimum (Fig. 1C). To verify the relevance of our findings, we used a 3D FIB/SEM tomography approach to image trophoblasts extracted from pregnant mice infected with *B. melitensis*. The data indicate that, similar to what is seen upon infection of HeLa cells by *B. abortus*, *B. melitensis* are contained in rBCVs, mostly as single bacteria. rBCVs are apparently expanded and remodeled rapidly to cover the surface of the individual bacteria present in the exponentially growing intracellular microcolony (Fig. 1D,E).

FIB/SEM tomography reveals extensive interactions between rBCVs and other host cell membranes

The ultimate advantage of FIB/SEM tomography compared to traditional EM approaches is the ability to image many consecutive layers at a resolution that allows membrane compartments of large 3D-volumes to be reconstructed. By using the tomograms, we could trace the interactions between BCVs and other organelles across the entire cytoplasmic volume of the infected host cell. Single tomogram frames indicated that the membrane of some BCVs form narrow protrusions that vary in shape and length. We were able to follow these protrusions across the consecutive tomogram slices, revealing their arrangement and connections with membranes located in their proximity (Fig. 2). 3D reconstructions demonstrated that some of the protrusions extend into ER cisternae. These structures were continuous with the rest of the ER, indicating that at least some of the bacteria are located directly in the ER lumen (Fig. 2A,B; Movie 1). We also detected extensions of rBCVs that formed vesicle-rich interfaces in the proximity of Golgi structures (Fig. 2C,D). This arrangement of membranes is reminiscent of previously described ER exit sites, which suggests that the vacuoles are continuous with functional ER (Zeuschner et al., 2006).

When rBCVs were located in the proximity of the nucleus, some of the extensions were continuous with membranes originating from the outer nuclear membrane (Fig. 2E,F). In some cases, the bacteria were found growing directly in the perinuclear space, with the outer nuclear membrane stretching to accommodate them (Fig. 2G,H). This phenomenon seemed to coincide with advanced stages of intracellular growth, when a large fraction of intracellular membranes had already been recruited to rBCVs.

Journal of Cell Science (2018) 131, jcs210799. doi:10.1242/jcs.210799

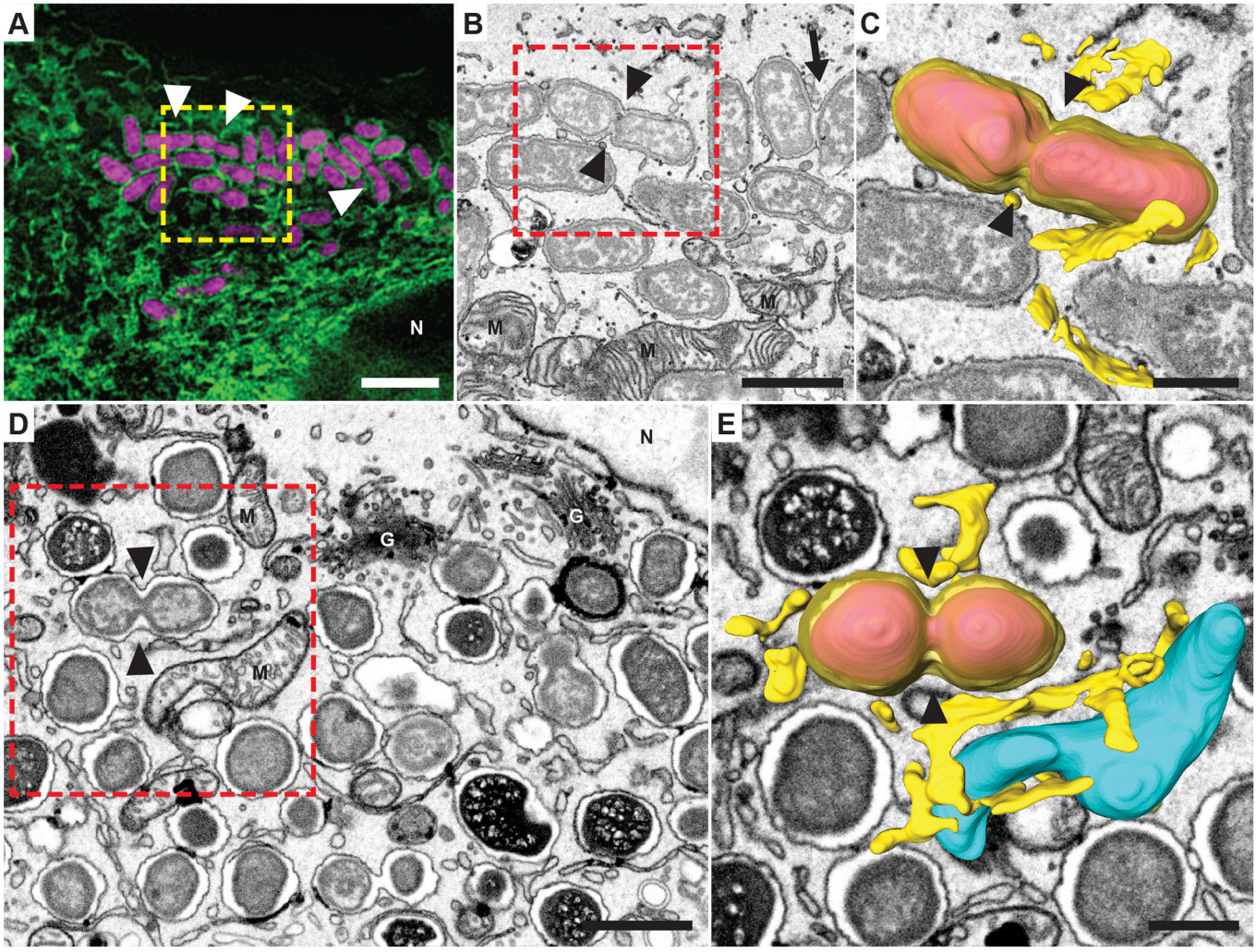

Fig. 1. Three-dimensional structure of the rBCV revealed with correlative FIB/SEM tomography. (A) SIM microscopy of a HeLa cell expressing the ER marker Emerald–Sec61β (green), infected with *B. abortus* expressing dsRed (magenta). Emerald–Sec61β staining circumscribes bacteria and localizes to adjacent ER cisternae. Some of the bacteria are undergoing division (arrowheads). The yellow box indicates an area that was later imaged using FIB/SEM. (B) Single image from a FIB/SEM tomogram depicting the area marked in A. rBCVs are seen as confined, single-membrane vacuoles. The BCVs containing dividing bacteria tighten next to the division septum formed as the daughter cells separate (arrowheads). Some rBCVs are occupied by more than one bacterium (arrow). The red box indicates the rBCV shown as a 3D reconstruction in C. (C) 3D reconstruction of the site marked in B, showing the rBCV membrane and adjacent ER cisternae (yellow). The dividing bacteria (pink) are efficiently enclosed by the rBCV membrane, which tightens around the septum formed as cell division progresses (arrowheads). (D) Single section from a FIB/SEM tomogram of a mouse trophoblast, at 5 days post infection (dpi) with *B. melitensis*. Large areas of the cell are filled with dividing bacteria. The red box indicates the rBCV that is shown in 3D in E. (E) 3D reconstruction of the site marked in D. The rBCV and neighboring ER structures are shown in pink and yellow, mitochondria are shown in cyan. Similar to what occurs with *B. abortus* in C, cell division is followed by fission of the rBCV (arrowheads) eventually giving rise to daughter cells residing in separate rBCV subcompartments. M, mitochondria; G, Golgi stacks; N, nucleus. Scale bars: 3 µm (A); 1 µm (B,D); 500 nm (C,E).

We also detected non-continuous contact sites between rBCVs and other membranous compartments. Interestingly, in some cases, we noticed slight deformations of the rBCV surface at sites where the membranes were touching (Fig. 2I), which could indicate the engagement of tethering factors that keep the two bilayers in close proximity. When visualized in 3D, the membranes were found to be parts of ER cisternae (Fig. 2J). The apparent prevalence of such contacts found within the host cell indicates that they might represent fusion and fission intermediates of the continuous connections discussed earlier.

The 3D information also allowed us to look at the level of continuity between rBCVs. Closer analysis of the tomograms revealed several sites where the membranes of neighboring rBCVs appeared to be continuous, resulting in assemblies of bacteria sharing the same organelle. These connections, however, were often only at certain points, with most of bacterial surface being surrounded by separated rBCV membranes (Fig. 2K,L).

3D-CLEM demonstrates that rBCVs are continuous with genuine ER

In order to unmistakably demonstrate the ER nature of membranes that were continuous with the rBCVs, we explored the full detail of our 3D-CLEM approach in 3D reconstructions of large parts of the host cell (Fig. 3A,B). Flat cisternae identified across the host cell volume (Fig. 3B) were found to be part of a network of interconnected membranes that originate from the outer nuclear membrane (Fig. 3C, bottom). An overlay of the two 3D volumes generated from the SIM and FIB/SEM data, respectively, indicated

Journal of Cell Science (2018) 131, jcs210799. doi:10.1242/jcs.210799

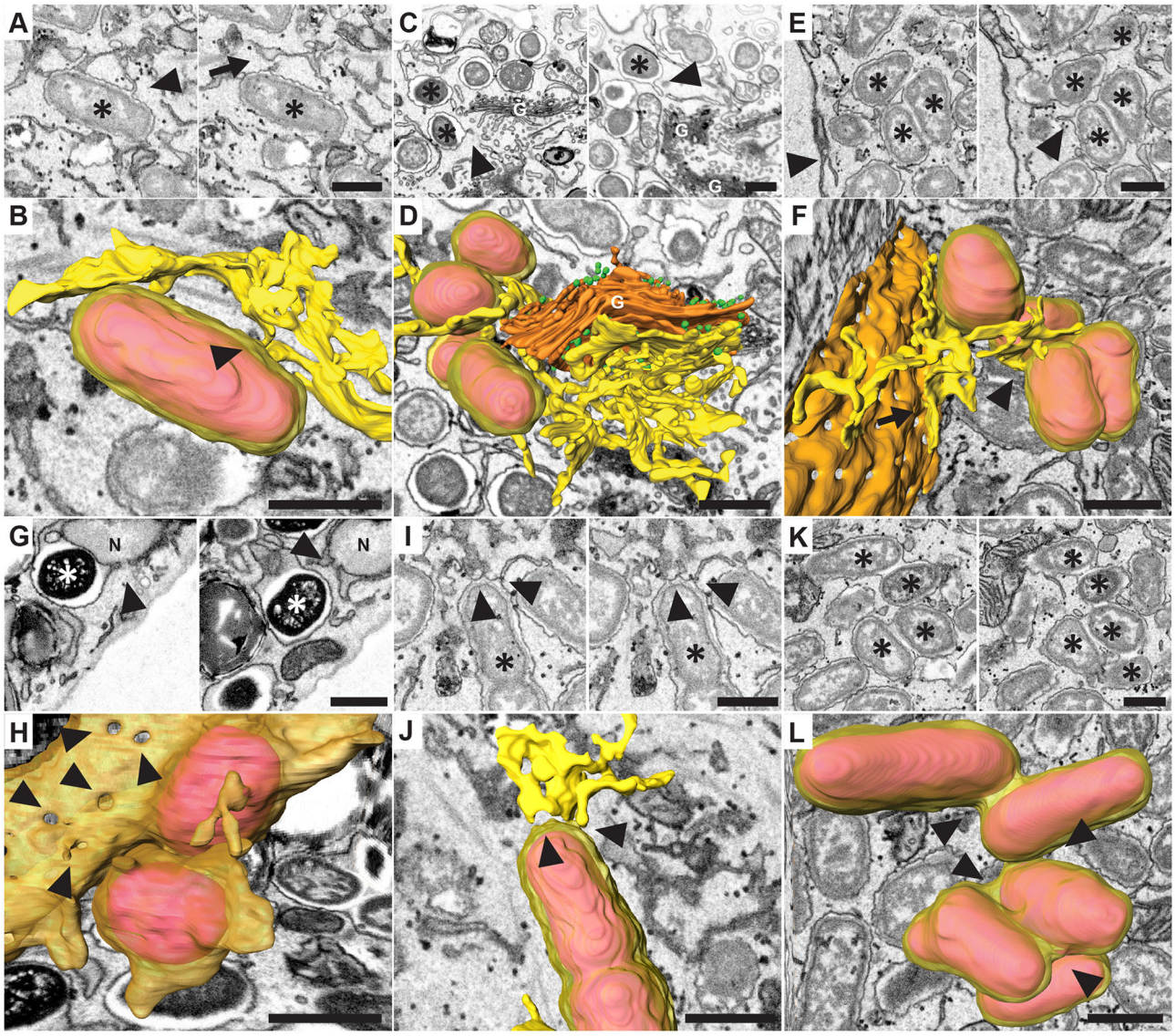

Fig. 2. Interactions between BCVs and organelles revealed by 3D FIB/SEM. (A) FIB/SEM of a HeLa cell infected with *B. abortus* at 24 hours post infection (hpi). Consecutive *z*-planes from a tomogram show a single rBCV (asterisk). Small protrusions can be observed originating from the surface of the vacuoles (left panel, arrowhead). The protrusion indicated was found to be continuous with the surrounding ER cisternae (right panel, arrow) upon examination of the entire 3D stack. (B) 3D reconstruction of the site in A reveals that the rBCV forms a connection (arrow) with the neighboring organelle membranes, which are a part of an extended ER mesh. (C) Images from a FIB/SEM tomogram of a mouse trophoblast at 5 days post infection (dpi) with *B. melitensis*. The rBCV has extensions (arrowheads) that were traced across the tomogram and found to be continuous with other host membranes. (D) 3D reconstruction of the site from C. The protrusions of the rBCVs (yellow) are continuous with a mesh of host ER membranes (yellow). The membranes form an interface with a Golgi stack (orange). A number of vesicles (green) are clustered at the interface and around the Golgi stack. (E) FIB/SEM of a HeLa cell infected with *B. abortus* at 24 hpi. Two different *z*-planes (heights) of the same site in a FIB/SEM stack are shown. A protrusion from a BCV (left panel, arrowhead) is continuous with an ER cisterna that originates from the outer nuclear membrane (right panel, arrowhead). (F) 3D reconstruction of the site from E showing four bacteria (pink) located in a large rBCV that is continuous with ER cisternae (arrowhead) originating from the outer nuclear membrane (orange, arrow). (G) Images from a FIB/SEM tomogram of a mouse trophoblast at 5 dpi with *B. melitensis*. The rBCVs visible in the images (asterisks) are continuous with the outer nuclear membrane of the host cell. Nuclear pore complexes (NPCs) are marked with arrowheads. (H) 3D reconstruction of the site from G indicates that the bacteria (pink) are located in an extension of the nuclear envelope (yellow). NPCs are marked with arrowheads. (I) FIB/SEM of a HeLa cell infected with *B. abortus* at 24 hpi. One of the rBCVs (asterisk) has several contact sites with surrounding ER cisternae (arrowheads). In some cases, we observed protrusions of the BCV membrane, indicating potential tethering between the lipid bilayers. (J) 3D reconstruction of the site depicted in I. The tethered membranes (yellow) are ER cisternae that share contact sites (arrowheads) with the BCV (yellow). (K) FIB/SEM of a HeLa cell infected with *B. abortus* at 24 hpi. Consecutive *z*-planes from a tomogram show a group of rBCVs (asterisks). The membrane of the BCVs is continuous (arrowheads), resulting in several bacteria being located in the same lumen. (L) 3D reconstruction of the site depicted in K. All the indicated bacteria (pink) are located in a large, continuous rBCV (yellow), connected by narrow extensions of the membrane (arrowheads). N, nucleus. Scale bars: 600 nm.

that the membranous cisternae colocalize with the signal from Emerald–Sec61β, which confirms that they are a part of the ER mesh spanning across the host cell (Fig. 3C, middle). Many rBCVs in a given area were connected to both each other and ER structures, constituting a part of this network (Fig. 3C). We were also able to resolve the fluorescence signal for some of the ER structures that formed direct connection with the rBCVs in the tomograms (Fig. 3D).

Journal of Cell Science (2018) 131, jcs210799. doi:10.1242/jcs.210799

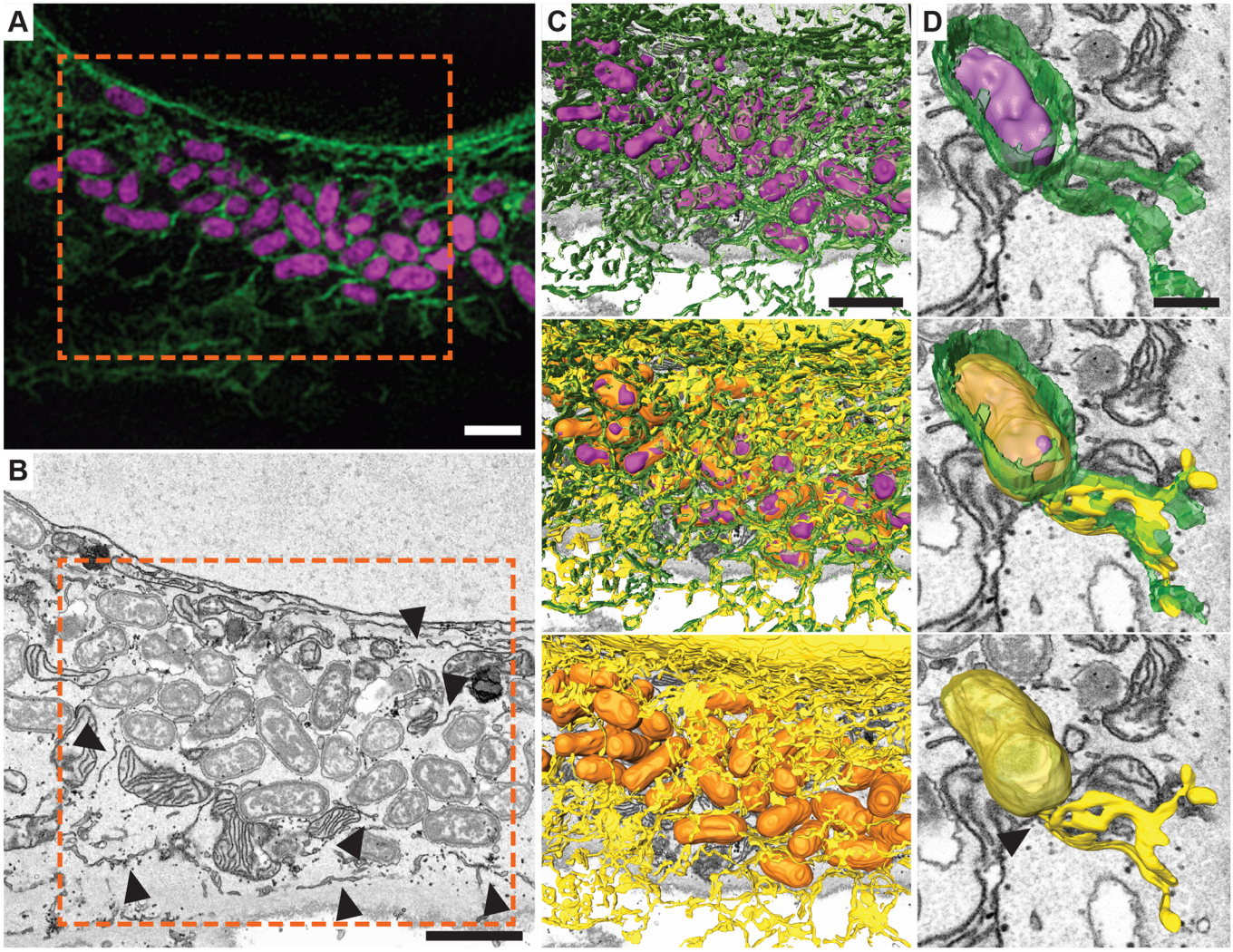

Fig. 3. CLEM reveals that BCV extensions colocalize with Emerald–Sec61β. (A) SIM image of a HeLa cell expressing Emerald–Sec61β infected with *B. abortus* expressing dsRed for 24 h. The bacteria (magenta) are dividing inside Sec61β-positive rBCVs (green). The resolution allows the ER mesh located in the proximity of the rBCVs to be distinguished. The marked area was imaged by FIB/SEM tomography. (B) Single frame from a FIB/SEM tomogram of the site marked in A showing stretches of flat cisternae distributed between the rBCVs (arrowheads). (C) 3D reconstruction of the site marked in B. Volumes generated by SIM (top) and FIB/SEM (bottom). Reconstruction of the SIM data, showing bacteria (magenta) and Sec61β-positive structures (green). The FIB/SEM reconstruction reveals the location of rBCVs (orange) and the ER, including the nuclear envelope (yellow). The two volumes were superimposed (middle) to indicate the colocalization of the Sec61β–GFP marker with the ER structures as well as the rBCV membranes. (D) One rBCV from C displayed with the same color code. Extensions of the BCV membrane are continuous with ER cisternae (arrowheads). The ER characteristic of the membranes reconstructed from the FIB/SEM tomogram (yellow), is confirmed by the superimposed Sec61β–GFP signal from SIM microscopy (middle). Scale bars: 1.5 µm (A–C); 500 nm (D).

The replicative niche of *Brucella* constitutes a complex 3D mesh with numerous connections to other host membranous compartments

After applying 3D-CLEM to explicitly demonstrate the continuity of rBCV membranes with the ER, our next aim was to quantify the level of networking by analyzing larger volumes of non-correlative FIB/SEM datasets (Fig. 4). In HeLa cells infected with *B. abortus*, we observed that many rBCVs were connected to ER cisternae that stretched across large distances (Fig. 4A,B). When the continuity between neighboring rBCVs was also taken into account, we found that a large portion of the vacuoles was integrated into the ER network. However, the exact level of connectivity between the rBCVs and the ER was difficult to quantify as there are many sites in the tomograms where the continuity of the membranes is questionable due to the resolution of the FIB/SEM tomograms (Fig. S2). In particular, the ER structures of HeLa cells displayed great variability in diameter and it was particularly difficult to judge the continuity of some fine cisternae (Fig. S2A). In mouse trophoblasts, the ER cisternae are in general more spacious and thus better suited to identify sites of continuity with rBCVs (Fig. S2B). Nevertheless, the following quantifications probably systematically underestimate the level of inter-connectivity. In HeLa cells, 57% (±2%; n=3) of bacteria were found to be located inside rBCVs that were continuous with the ER. In the case of mouse trophoblasts infected with *B. melitensis*, the proportion was 71% (±8%; n=3) (Fig. 4C,D). The results suggest that in both cases most bacteria reside inside BCVs that are integrated into the ER meshwork.

After post-division separation of bacteria, continuity between BCVs is limited to small surface areas

As shown above, bacteria residing in rBCVs are not only connected to the ER lumen, but often also straight to neighboring rBCVs. We

Journal of Cell Science (2018) 131, jcs210799. doi:10.1242/jcs.210799

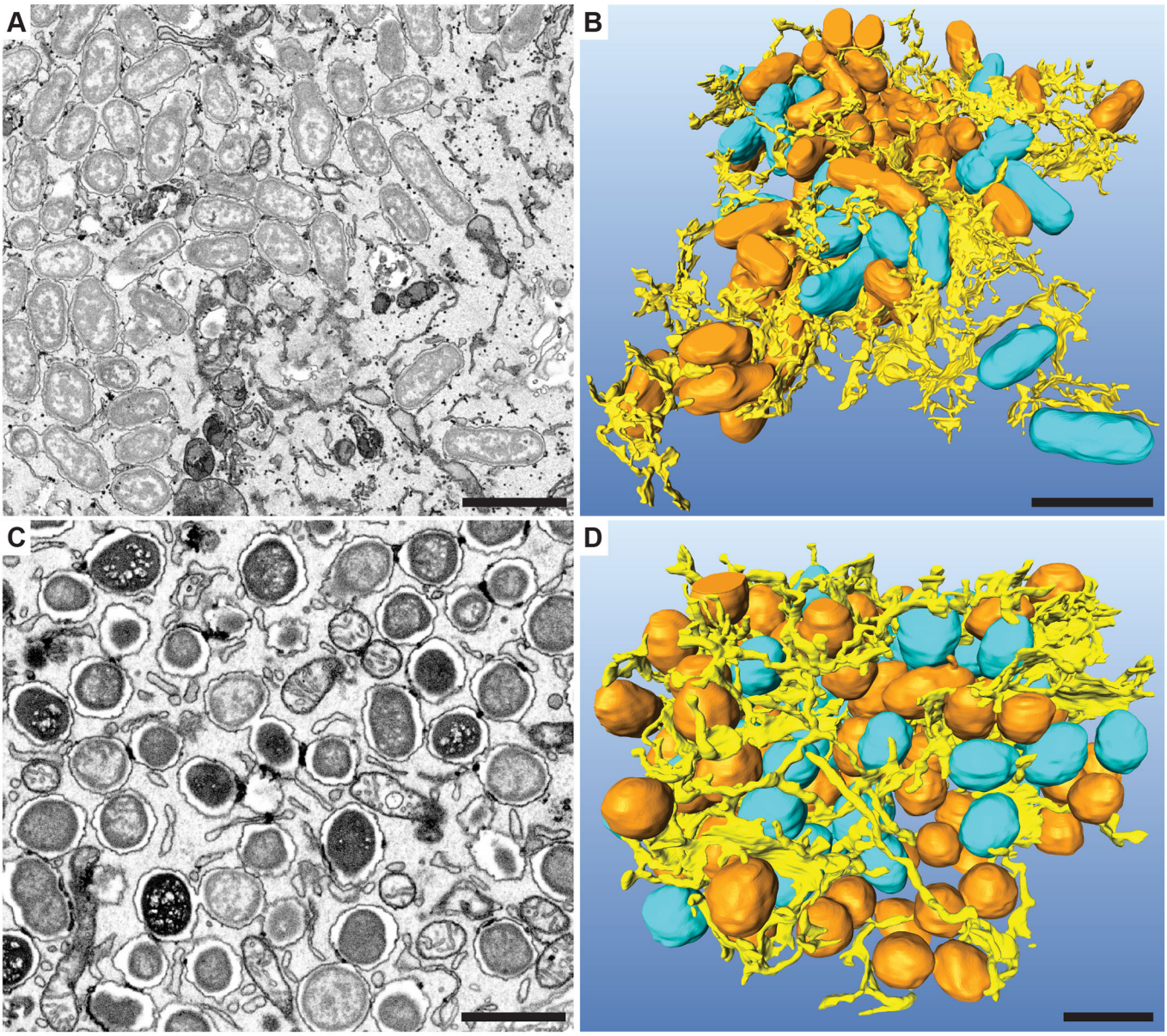

Fig. 4. The replicative niche of *Brucella* constitutes an extended complex compartment that spans large volumes of the host cell. (A) Single frame from a FIB/SEM tomogram of a HeLa cell infected with *B. abortus* at 24 hours post infection (hpi). Most of the bacteria appear to be located in individual single-membrane rBCVs. (B) 3D reconstruction of the FIB/SEM tomogram from A. ER membranes (yellow) form an extended mesh that surrounds the rBCVs (orange and cyan). A large proportion of the rBCVs (orange) are continuous with the ER cisternae, sharing a common lumen with the entire ER network. rBCVs for which the connection was not visible in the EM data are colored in cyan. (C,D) Similar to A,B, but the FIB/SEM data depicts a mouse trophoblast infected with *B. melitensis* at 5 days post infection (dpi). The ER mesh forms connections with many of the rBCVs (orange), indicating that the vacuoles are to a large extent continuous with the ER network. Scale bars: 1.5 µm (A,B); 1 µm (C,D).

wondered whether these direct connections between rBCVs are the result of incomplete post-division separation or whether they, at least in part, reflect fusion events between distinct rBCVs. In search for the latter, we examined the structure of the replicative niche in HeLa cells that were co-infected with two strains of *B. abortus*, each expressing a different fluorescent marker (Fig. 5). Confocal analysis of HeLa cells expressing Emerald–Sec61β showed that occasionally cells are infected by both strains, resulting in mixed microcolonies (Fig. 5A). The level of spatial overlap between bacteria of the two strains varied from cell to cell, suggesting that it might simply depend on the random distribution of bacteria relative to each other at the point when the replicative niche is established.

Our correlative approach allowed us to distinguish both strains in FIB/SEM tomograms (Fig. 5B). We were able to find cases of continuity between rBCVs occupied by bacteria belonging to different lineages, suggesting fusion between the vacuoles. Such connections, however, were always limited to small surface areas. The presence of two bacteria inside the bulk volume of the same rBCV was only observed for bacteria from the same lineage, thus likely representing post-division cells (Fig. 5C). As expected, rBCVs containing individual bacteria from both lineages were found to be connected to ER cisternae and thus to constitute integral parts of the ER network (Fig. 5D).

Journal of Cell Science (2018) 131, jcs210799. doi:10.1242/jcs.210799

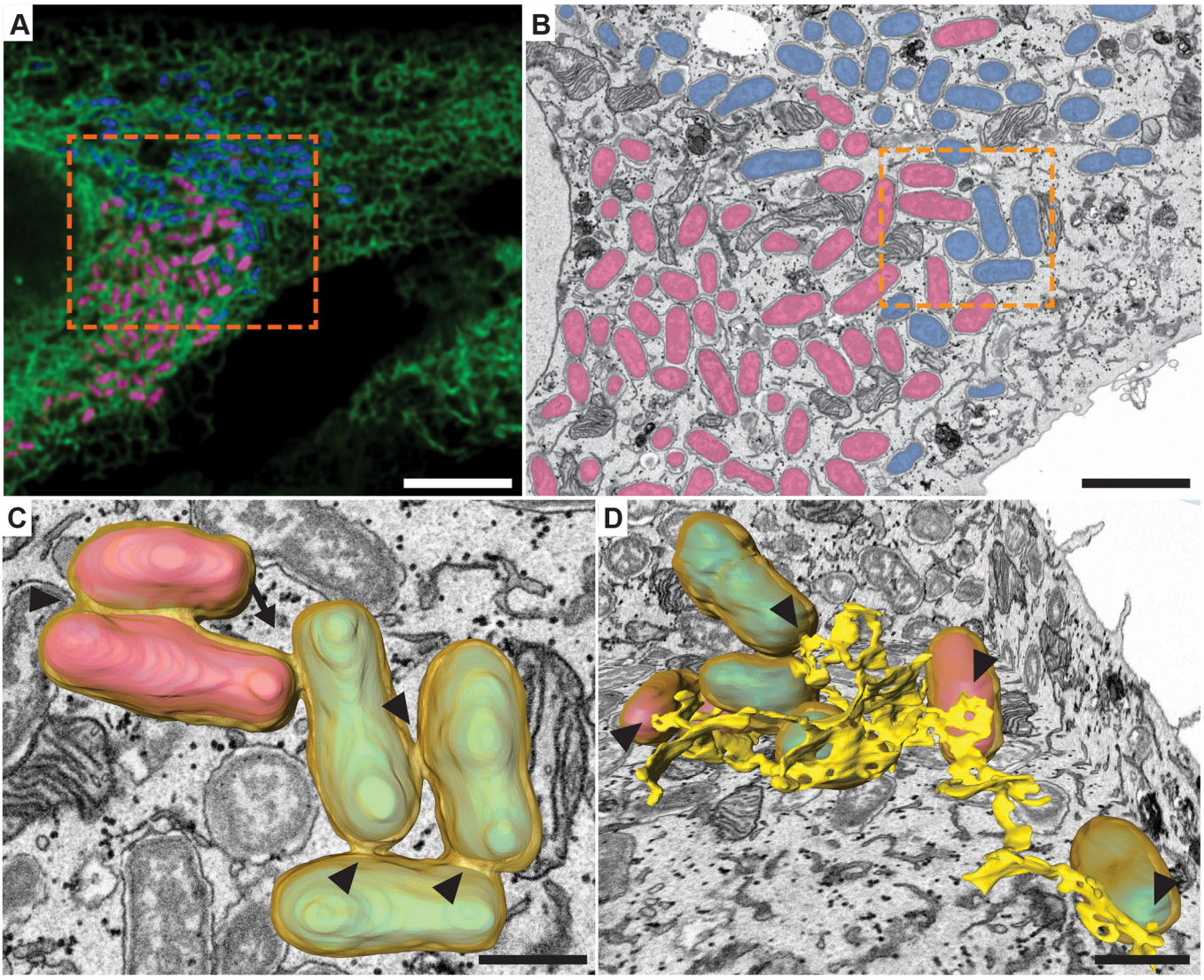

Fig. 5. rBCVs undergo limited fusion. (A) Confocal microscope image of HeLa cell expressing Emerald–Sec61β (green), co-infected with *B. abortus* expressing BFP (blue) and *B. abortus* expressing dsRed (pink) at 24 hours post infection (hpi). Bacteria are located inside Sec61β-positive compartments. The marked area was imaged using FIB/SEM. (B) Single image from a FIB/SEM tomogram of the site marked in A. Bacteria were colored pink or blue based on the confocal data, depending on which of the two strains they represent. (C) 3D reconstruction of the site marked in B, including bacteria from both strains. There is membrane continuity between rBCVs belonging to the same (arrowheads) or different strains (arrow), although the latter kind of connection is limited to small surfaces. (D) 3D reconstruction depicting several BCVs (blue or pink bacteria visible inside) and parts of the ER mesh (yellow) across the FIB/SEM tomogram. All BCVs present in the reconstruction were found to be continuous with the same network of ER cisternae (arrowheads), constituting a single extended organelle. Scale bars: 6 µm (A); 2 µm (B); 700 nm (C,D).

DISCUSSION

Several intracellular pathogens are known to thrive inside vacuoles that display at least some characteristics of host cellular organelles (Celli and Tsolis, 2015). Once it has been successfully established, a vacuolar replicative compartment requires constant remodeling through membrane fusion and fission events in order to facilitate the evasion of host cell defenses, the acquisition of nutrients, and volume and shape changes to adjust to pathogen growth. EM has provided invaluable information about the ultrastructural details of such pathogen-containing vacuoles inside host cells (Celli et al., 2003; Robinson and Roy, 2006; Starr et al., 2012; Tilney et al., 2001). Most studies, however, are based on flat ultrathin sections, which fail to resolve the 3D membrane assemblies of cellular organelles and their complex interactions. The facultative intracellular pathogen *Brucella* is an interesting example in this respect. Ultrastructural analysis in combination with cell biology studies has suggested a relationship between the rBCV and the ER (Celli et al., 2003; Detilleux et al., 1990a). However, the lack of 3D ultrastructural information has hampered a thorough characterization of the role of the ER in establishing and maintaining rBCVs. By combining FIB/SEM tomography with SIM super-resolution fluorescent imaging, we were able to visualize the complex structure of the ER and its interactions with rBCVs formed by two species of brucellae, *B. abortus* and *B. melitensis*, in human and mouse cells, respectively.

Our FIB/SEM data indicate that seemingly isolated rBCVs are often connected to other rBCVs as well as to extended membranous cisternae. We demonstrated that these membranes can be traced back to the outer nuclear membrane in the reconstructed 3D volumes. Moreover, by correlating fluorescent SIM data with EM,

Journal of Cell Science (2018) 131, jcs210799. doi:10.1242/jcs.210799

we could demonstrate that the marker GFP–Sec61β colocalizes with both the rBCVs of *B. abortus* and the membranes that are continuous with them. This confirms that, at a given time, some of the rBCVs share a continuous lumen with the ER. These observations in infected HeLa cells, were confirmed by FIB/SEM imaging of trophoblasts in the placenta of pregnant mice infected with *B. melitensis*. Similar to *B. abortus* in HeLa cells, the rBCVs were often found to be connected directly to ER cisternae and the outer nuclear membrane.

Not all rBCVs in a given cell volume were found to be integrated into the ER network. In part, this may result from technical limitations of the FIB/SEM tomography approach, as this method does not allow all membranous structures to be resolved and thus systematically underestimates connectivity. However, incomplete continuity between rBCVs and ER may also reflect dynamic remodeling that constantly takes place within the ER (Nixon-Abell et al., 2016). In agreement, the numerous seemingly discontinuous contact sites between rBCVs and the ER observed in addition to direct membrane continuity most likely reflect tethering events between these compartments. We speculate that they may be snapshots of dynamic fusion or fission events responsible for the assembly and disassembly of connections between rBCVs and the remaining ER volume. Apparent continuity between rBCVs containing bacteria of two distinct strains in co-infected cells, indicates that they dynamically undergo fusion with other rBCVs and possibly also with distant ER structures.

A striking characteristic of rBCVs is the tight wrapping of individual bacteria by the host-derived membranes. During intracellular infection, bacteria numbers double roughly every 3 h (Gamazo et al., 1993) until a large portion of the host cytoplasm is occupied by rBCVs. Segregation of dividing bacteria by host membranes is fast and efficient. Even by late stages of bacterial division – before the separation of daughter cells is completed – the rBCV membranes invaginate at the site of septation. Homotypic fusion of rBCVs to produce large vacuoles containing multiple bacteria was hardly ever observed. Thus, the overall membrane surface area of the rBCVs seems to be higher than for most other intracellular bacteria, which do typically grow in more spacious vacuoles that accommodate multiple bacteria (Case et al., 2016). This suggests that substantial amounts of membrane must be recruited to keep bacteria in relatively confined spaces. If the replicative niche indeed represents stretched ER cisternae, as indicated by our findings, it seems that the volume of the organelle is kept to a minimum at the cost of generating more membrane surface. We speculate that rBCVs undergo fusion and fission events that are orchestrated by host factors normally responsible for the remodeling of the ER (English and Voeltz, 2013; Nixon-Abell et al., 2016). It has been shown that one of the ways of alleviating ER stress is the expansion of cisternae volume through lipid biosynthesis (Schuck et al., 2009). In future experiments, it would thus be interesting to test whether the presence of *Brucella* inside the ER network triggers this or other mechanisms to increase the membrane surface.

It will also be important to clarify whether these processes of membrane expansion in the replicative niche require active signaling by bacteria or are merely a consequence of physical forces caused by growing bacteria. It is well established that the T4SS and possibly its effectors are required for the formation of the rBCV (Comerci et al., 2001). Recent evidence suggests that the effector BspB is needed for efficient division of *Brucella* in the rBCV (Miller et al., 2017). Additionally, the effector VceC has been shown to cause ER stress via triggering of the unfolded protein response (UPR) (Keestra-Gounder et al., 2016; Wang et al., 2016). However, both these effectors play only modulatory roles as they are not essential for rBCV expansion. Moreover, there is evidence that T4SS inactivation in bacteria residing already within an rBCV has limited influence on the rate of *Brucella* replication (Smith et al., 2016). Although we cannot rule out the activity of yet unidentified T4SS-independent factors, these data may suggest that, following initial entry into the ER lumen, bacteria may not need to actively induce membrane acquisition in order to expand the rBCV.

Together, the data support the hypothesis that following entry and initial trafficking along the endocytic network, *Brucella* escapes into the ER lumen, rather than isolated ER-derived vacuoles, to establish its replicative niche. This allows the pathogen not only to use nutrients contained within the extended ER network, but also to rely on homeostatic mechanisms of membrane expansion and structure to sustain bacterial growth. Further studies of the replicative niche will provide details about the unique interactions of *Brucella* with the ER, and might also shed new light on the fundamental cellular processes responsible for controlling the structure and metabolism of the ER.

MATERIALS AND METHODS

Bacteria strains and plasmids

The plasmid pJC44 encoding the DsRed gene was a kind gift from Jean Celli (Washington State University, Pullman, WA) (Starr et al., 2008). The plasmid pJS17 encoding Tet-DsRed and mTagBFP2 was generated from pAC042.08 (Casanova et al., 2016) by replacing the GFP cassette with DsRed for inducible expression, and the DsRed cassette with mTagBFP for constitutive expression. Both plasmids were conjugated into *B. abortus* strain 2308. *B. melitensis* strain 16 M (Biotype1, ATCC 23,456) carrying the plasmid pKSoriT-bla-kan-PsojA-mCherry has been described previously (Copin et al., 2012).

Mammalian cell lines and plasmids

The HeLa human cervical carcinoma epithelial cell line (ATCC, CCL-2) was maintained in Dulbecco's modified Eagle's medium (DMEM) supplemented with 10% fetal calf serum (FCS). The plasmid carrying the Sec61β–Emerald construct containing an Emerald–GFP gene followed by Sec61β was a kind gift from Jennifer Lippincott-Schwartz (National Institute of Health, Bethesda, MD) (Nixon-Abell et al., 2016). The plasmid carrying the calnexin–GFP gene was a kind gift from Gisou van der Goot (Global Health Institute, EPFL, Lausanne, Switzerland) (Lakkaraju et al., 2012). Plasmids MDK124-Emerald-Sec61β and MDK124-GFP-calnexin were generated by cloning the respective constructs into the pMDK124 vector using the EcoRI and BamHI restriction sites. The plasmids were then used for lentivirus generation and transduction of HeLa cells. Cell lines were routinely tested for contamination with a PCR mycoplasma test kit (Applichem).

Mammalian cell culture infection

HeLa cells were seeded onto 32 mm gridded glass coverslips (Ibidi, Martinsried, Germany) in a six-well plate at 150,000 cells per well and incubated overnight. *B. abortus* 2308 strains carrying either pJC44 or pJS17 were grown overnight in trypticase soy broth (TSB) medium containing 50 µg/ml kanamycin at 37°C to an optical density (OD) of 0.8–1.0. Bacteria were then diluted in DMEM with 10% FCS and added to HeLa cells at a final multiplicity of infection (MOI) of 2000. Plates were centrifuged at 400 ***g*** for 20 min at 4°C to synchronize bacterial entry. After 2 h of incubation at 37°C and 5% CO_2, extracellular bacteria were killed by exchanging the infection medium to DMEM with 10% FCS supplemented with 100 µg/ml gentamicin. After the total infection time indicated in the figure legends, cells were fixed using PHEM fixation buffer (4% formaldehyde, 0.2% glutaraldehyde, 60 mM PIPES, 25 mM HEPES, 10 mM EGTA and 4 mM $MgCl_2$) for 90 min at room temperature. Following fixation, the coverslips were washed in PHEM buffer (60 mM PIPES, 25 mM HEPES, 10 mM EGTA and 4 mM $MgCl_2$) and mounted onto 38 mm glass slides (BioSystems, Muttenz, Switzerland) using

Vectashield H1000 mounting medium (Vector Laboratories, Burlingame, CA) and sealed with nail polish.

Fluorescence microscopy

3D-SIM was performed using a DeltaVision OMX-Blaze system (version 4; GE Healthcare) equipped with 488 and 568 nm solid-state lasers, a Plan Apo N 63×, 1.42 NA oil objective and four liquid-cooled sCMOs cameras (pco Edge, full frame 2560×2160; Photometrics), or a Zeiss Elyra S.1 microscope (Carl Zeiss, Oberkochen, Germany) equipped with a Andor iXon 885 EMCCD camera, HR diode 488 nm and 561 nm 100 nW solid state lasers and a Plan Apo 63× NA 1.4 oil objective. For OMX-Blaze, optical *z*-sections were separated by 0.125 µm. Exposure times were between 3 and 10 ms, with three rotations of the illumination grid. Multichannel imaging was achieved through sequential acquisition of wavelengths by separate cameras. First, the channels were aligned in the image plane and around the optical axis using predetermined shifts measured using a target lens and the SoftWoRx alignment tool. Afterwards, they were carefully aligned using alignment parameters from control measurements made with 0.5 µm diameter multi-spectral fluorescent beads (Invitrogen, Thermo Fisher Scientific). Raw 3D-SIM images were processed and reconstructed using the DeltaVision OMX SoftWoRx software package (GE Healthcare) (Gustafsson, 2000). The final voxel size was 40 nm×40 nm×125 nm. For Zeiss Elyra, cells were sectioned at 0.13 µm intervals taken at 50 ms exposures per slice with three rotations of the illumination grid. Zen Black software (Carl Zeiss) was used to process the images using automatic settings but retaining the raw scale. Confocal images were acquired with a LSM 800 confocal microscope (Carl Zeiss) using a 63× oil objective. Grid coordinates of imaged cells were saved for correlation with electron microscopy. Following image acquisition, coverslips were detached from slides and fixed in cacodylate fixation buffer (2.5% glutaraldehyde, 150 mM sodium cacodylate, 2 mM $MgCl_2$) at 4°C overnight.

Mouse infection and organ collection

The procedures used in this study and the handling of the mice complied with current European legislation (directive 86/609/EEC) and the corresponding Belgian law 'Arrêté royal relatif à la protection des animaux d'expérience du 6 Avril 2010 publié le 14 Mai 2010'. The Animal Welfare Committee of the University of Namur (Namur, Belgium) reviewed and approved the complete protocol (Permit Number 16/277). Bacterial growth of *B. melitensis* cultures was measured through the culture optical density at 600 nm. Bacterial cultures were spun down, washed with RPMI medium (Gibco) and resuspended for injection in the same medium at a density of 2×10^5 CFU/ml. The estrous cycle of 8–14-week-old BALB/c females was synchronized 3 days before mating and pairs were set up with 3- to 4-month-old males. The following morning, the presence of a vaginal plug was checked and the potentially fertilized females were isolated. That day corresponded to day 0 post-fecundation (PF). At day 10 PF, pregnant females were infected intraperitoneally with 500 µl of bacterial suspension (10^5 bacteria). At day 15 PF, mice were anesthetized with isoflurane and killed by cervical dislocation, as previously described (Barbier et al., 2017). All infections were performed at an Animal Biosafety Level 3 facility. Conceptuses were removed from maternal uterine horns and fixed overnight at 4°C in PBS supplemented with 2.5% glutaraldehyde. Tissue fragments were washed several times in cacodylate buffer (150 mM sodium cacodylate, 2 mM $MgCl_2$) at 4°C. The samples were then fixed overnight in 2.5% glutaraldehyde in cacodylate buffer (150 mM sodium cacodylate, 2 mM $MgCl_2$) at 4°C.

Electron microscopy sample preparation

Both cell monolayers and placenta fragments were processed for electron microscopy using the same protocol. Following overnight fixation, samples were washed three times with cacodylate buffer (150 mM sodium cacodylate, 2 mM $MgCl_2$) at 4°C. They were then immersed in freshly prepared reduced osmium buffer (2% osmium tetroxide, 150 mM sodium cacodylate, 2 mM $MgCl_2$, 40 mM potassium ferrocyanide) for 1 h at 4°C. After this initial staining/fixation step, the samples were washed with deionized water at room temperature and immersed in 100 mM thiocarbohydrazide solution for 20 min at room temperature. They were then washed with deionized water and incubated in 2% osmium tetroxide for 30 min at room temperature. This was followed by overnight incubation in 1% uranyl acetate at 4°C. The following morning, the samples were washed in deionized water and incubated in freshly prepared 20 mM lead aspartate solution for 30 min at 60°C. They were then dehydrated with ethanol and immersed in 50% solution of durcupan in ethanol for 1 h. Afterwards, the samples were incubated two times in fresh durcupan and placed at 60°C for 48 h for polymerization.

Focused ion beam scanning electron microscopy

For cell monolayers, the cells of interest were located in the polymerized resin block, trimmed and attached to pre-tilt 45° SEM stubs (Agar Scientific, Stansted, UK) using colloidal silver paint (Ted Pella, Redding, CA), sputter-coated with platinum and subjected to FIB/SEM tomography. For placenta samples, the resin blocks were cut into small pieces and mounted to flat SEM stubs (Ted Pella, Redding, CA). The blocks were then processed using the EM UC7 microtome (Leica, Wetzlar, Germany). The blocks were initially polished with a glass knife and then a series of 70 nm ultrathin sections was cut using a diamond knife (Diatome, Nidau, Switzerland). Cells carrying bacteria were located in the ultrathin sections using a T12 TEM (FEI, Hillsboro, OR). The corresponding locations were found in the resin blocks and imaged by FIB/SEM. The images were acquired with a Helios NanoLab 650 Dual Beam FIB/SEM using the Slice and View software (FEI, Hillsboro, OR). They had 3072×2048 or 2048×1780 pixel and were collected using an Elstar in-lens BSE detector at 1.5 kV with a horizontal field width of 15 µm at a working distance of 4.01 mm. The milling was performed with a FIB operating at 30 kV and 0.78 nA beam current. The thickness of the slices was between 10 and 20 nm. Image stacks were aligned by using the TrackEM2 plugin for ImageJ (Cardona et al., 2010). Image analysis and quantification was performed using the IMOD software package (Kremer et al., 1996). For each bacterium, the corresponding rBCV membranes were analyzed for continuity with those of other rBCVs or ER cisternae across neighboring sections of the tomograms. For both HeLa cell and mouse placenta samples, three FIB/SEM volumes, each representing an area within an infected cell, were analyzed. The number of bacteria analyzed in each volume varied between 132 and 173 for HeLa cell samples and between 167 and 838 for mouse trophoblasts. The manual segmentations and 3D representations of the electron microscopy datasets were achieved using the FEI Amira software (FEI, Hillsboro, OR).

Acknowledgements

We are grateful to the Jean Celli (Washington State University, Pullman, WA) for providing the JC44 plasmid. We thank Dr Jennifer Lippincott-Schwartz for providing the Emerald-Sec61β construct. We thank Dr Gisou van der Goot for providing the calnexin–GFP construct. The authors acknowledge the technical assistance of Marcel Düggelin (ZMB, University of Basel, Switzerland) and Daniel Mathys (SNI, University of Basel, Switzerland) for the assistance with FIB/SEM imaging. We thank the Imaging Core Facility (IMCF, University of Basel, Switzerland) and in particular Alexia Ferrand for the technical assistance provided on the OMX microscope. We thank Laurent Gelman (Friedrich Miescher Institute, Basel, Switzerland) for the technical assistance provided with the Elyra microscope. We would like to thank Maxime Québatte for critical reading of the manuscript.

Competing interests

The authors declare no competing or financial interests.

Author contributions

Conceptualization: J.S., H.S., C.D.; Methodology: J.S., T.T., S.H.L., K.W., K.N.G., J.-J.L., H.S.; Investigation: J.S., T.T., S.H.L., K.W.; Writing - original draft: J.S., C.D.; Writing - review & editing: T.T., K.N.G., J.-J.L., H.S., C.D.; Visualization: J.S.; Supervision: K.N.G., J.-J.L., H.S., C.D.; Project administration: H.S., C.D.; Funding acquisition: J.-J.L., H.S., C.D.

Funding

This work was supported by the Schweizerischer Nationalfonds zur Förderung der Wissenschaftlichen Forschung (Swiss National Science Foundation; SNSF) (grant 31003A_173119 to C.D.); a European Research Council (ERC) advanced grant (FicModFun) (340330 to C.D.); the Research and Technology Development (RTD)

project TargetInfectX in the frame of SystemsX.ch (www.systemX.ch) to C.D. (grant 51RTP0_151029); the Swiss Initiative for Systems Biology; and by grant NCCR TransCure from the SNSF to H.S. The research at UNamur was supported by the Interuniversity Attraction Poles Program initiated by the Federaal Wetenschapsbeleid (Belgian Science Policy Office) (PAI no. P7/28).

Supplementary information

Supplementary information available online at
http://jcs.biologists.org/lookup/doi/10.1242/jcs.210799.supplemental

References

Alcantara, C. L., Vidal, J. C., de Souza, W. and Cunha, E. S. N. L. (2017). The cytostome-cytopharynx complex of *Trypanosoma cruzi* epimastigotes disassembles during cell division. *J. Cell Sci.* **130**, 164-176.

Anderson, T. D., Cheville, N. F. and Meador, V. P. (1986). Pathogenesis of placentitis in the goat inoculated with *Brucella abortus*. II. Ultrastructural studies. *Vet. Pathol.* **23**, 227-239.

Archambaud, C., Salcedo, S. P., Lelouard, H., Devilard, E., de Bovis, B., Van Rooijen, N., Gorvel, J.-P. and Malissen, B. (2010). Contrasting roles of macrophages and dendritic cells in controlling initial pulmonary *Brucella* infection. *Eur. J. Immunol.* **40**, 3458-3471.

Atluri, V. L., Xavier, M. N., de Jong, M. F., den Hartigh, A. B. and Tsolis, R. M. (2011). Interactions of the human pathogenic *Brucella* species with their hosts. *Annu. Rev. Microbiol.* **65**, 523-541.

Barbier, T., Machelart, A., Zúñiga-Ripa, A., Plovier, H., Hougardy, C., Lobet, E., Willemart, K., Muraille, E., De Bolle, X., Van Schaftingen, E. et al. (2017). Erythritol availability in bovine, murine and human models highlights a potential role for the host aldose reductase during *Brucella* infection. *Front. Microbiol.* **8**, 1088.

Bellaire, B. H., Roop, R. M., III and Cardelli, J. A. (2005). Opsonized virulent *Brucella abortus* replicates within nonacidic, endoplasmic reticulum-negative, LAMP-1-positive phagosomes in human monocytes. *Infect. Immun.* **73**, 3702-3713.

Boschiroli, M. L., Ouahrani-Bettache, S., Foulongne, V., Michaux-Charachon, S., Bourg, G., Allardet-Servent, A., Cazevieille, C., Liautard, J. P., Ramuz, M. and O'Callaghan, D. (2002). The *Brucella suis* virB operon is induced intracellularly in macrophages. *Proc. Natl. Acad. Sci. USA* **99**, 1544-1549.

Cardona, A., Saalfeld, S., Preibisch, S., Schmid, B., Cheng, A., Pulokas, J., Tomancak, P. and Hartenstein, V. (2010). An integrated micro- and macroarchitectural analysis of the *Drosophila* brain by computer-assisted serial section electron microscopy. *PLoS Biol.* **8**.

Casanova, A., Low, S. H., Emmenlauer, M., Conde-Alvarez, R., Salcedo, S. P., Gorvel, J. P. and Dehio, C. (2016). Microscopy-based assays for high-throughput screening of host factors involved in *Brucella* infection of HeLa cells. *J. Vis. Exp.* **114**, e54263.

Case, E. D. R., Smith, J. A., Ficht, T. A., Samuel, J. E. and de Figueiredo, P. (2016). Space: a final frontier for vacuolar pathogens. *Traffic* **17**, 461-474.

Celli, J. and Tsolis, R. M. (2015). Bacteria, the endoplasmic reticulum and the unfolded protein response: friends or foes? *Nat. Rev. Microbiol.* **13**, 71-82.

Celli, J., de Chastellier, C., Franchini, D.-M., Pizarro-Cerda, J., Moreno, E. and Gorvel, J.-P. (2003). *Brucella* evades macrophage killing via VirB-dependent sustained interactions with the endoplasmic reticulum. *J. Exp. Med.* **198**, 545-556.

Comerci, D. J., Martinez-Lorenzo, M. J., Sieira, R., Gorvel, J.-P. and Ugalde, R. A. (2001). Essential role of the VirB machinery in the maturation of the *Brucella abortus*-containing vacuole. *Cell. Microbiol.* **3**, 159-168.

Copin, R., Vitry, M.-A., Hanot Mambres, D., Machelart, A., De Trez, C., Vanderwinden, J.-M., Magez, S., Akira, S., Ryffel, B., Carlier, Y. et al. (2012). In situ microscopy analysis reveals local innate immune response developed around *Brucella* infected cells in resistant and susceptible mice. *PLoS Pathog.* **8**, e1002575.

Creasey, E. A. and Isberg, R. R. (2014). Maintenance of vacuole integrity by bacterial pathogens. *Curr. Opin. Microbiol.* **17**, 46-52.

Delevoye, C., Nilges, M., Dehoux, P., Paumet, F., Perrinet, S., Dautry-Varsat, A. and Subtil, A. (2008). SNARE protein mimicry by an intracellular bacterium. *PLoS Pathog.* **4**, e1000022.

Detilleux, P. G., Deyoe, B. L. and Cheville, N. F. (1990a). Entry and intracellular localization of *Brucella spp.* in Vero cells: fluorescence and electron microscopy. *Vet. Pathol.* **27**, 317-328.

Detilleux, P. G., Deyoe, B. L. and Cheville, N. F. (1990b). Penetration and intracellular growth of *Brucella abortus* in nonphagocytic cells in vitro. *Infect. Immun.* **58**, 2320-2328.

English, A. R. and Voeltz, G. K. (2013). Rab10 GTPase regulates ER dynamics and morphology. *Nat. Cell Biol.* **15**, 169-178.

Fratti, R. A., Chua, J., Vergne, I. and Deretic, V. (2003). Mycobacterium tuberculosis glycosylated phosphatidylinositol causes phagosome maturation arrest. *Proc. Natl. Acad. Sci. USA* **100**, 5437-5442.

Gamazo, C., Vitas, A. I., López-Goñi, I., Diaz, R. and Moriyón, I. (1993). Factors affecting detection of *Brucella melitensis* by BACTEC NR730, a nonradiometric system for hemocultures. *J. Clin. Microbiol.* **31**, 3200-3203.

Gustafsson, M. G. (2000). Surpassing the lateral resolution limit by a factor of two using structured illumination microscopy. *J. Microsc.* **198**, 82-87.

Gustafsson, M. G. L., Shao, L., Carlton, P. M., Wang, C. J. R., Golubovskaya, I. N., Cande, W. Z., Agard, D. A. and Sedat, J. W. (2008). Three-dimensional resolution doubling in wide-field fluorescence microscopy by structured illumination. *Biophys. J.* **94**, 4957-4970.

Gutierrez, M. G., Vázquez, C. L., Munafó, D. B., Zoppino, F. C., Beron, W., Rabinovitch, M. and Colombo, M. I. (2005). Autophagy induction favours the generation and maturation of the Coxiella-replicative vacuoles. *Cell. Microbiol.* **7**, 981-993.

Keestra-Gounder, A. M., Byndloss, M. X., Seyffert, N., Young, B. M., Chávez-Arroyo, A., Tsai, A. Y., Cevallos, S. A., Winter, M. G., Pham, O. H., Tiffany, C. R. et al. (2016). NOD1 and NOD2 signalling links ER stress with inflammation. *Nature* **532**, 394-397.

Knott, G., Rosset, S. and Cantoni, M. (2011). Focussed ion beam milling and scanning electron microscopy of brain tissue. *J. Vis. Exp.* **53**, e2588.

Kremer, J. R., Mastronarde, D. N. and McIntosh, J. R. (1996). Computer visualization of three-dimensional image data using IMOD. *J. Struct. Biol.* **116**, 71-76.

Lakkaraju, A. K. K., Abrami, L., Lemmin, T., Blaskovic, S., Kunz, B., Kihara, A., Dal Peraro, M. and van der Goot, F. G. (2012). Palmitoylated calnexin is a key component of the ribosome-translocon complex. *EMBO J.* **31**, 1823-1835.

Lestrate, P., Delrue, R.-M., Danese, I., Didembourg, C., Taminiau, B., Mertens, P., De Bolle, X., Tibor, A., Tang, C. M. and Letesson, J.-J. (2000). Identification and characterization of in vivo attenuated mutants of *Brucella melitensis*. *Mol. Microbiol.* **38**, 543-551.

Mellouk, N., Weiner, A., Aulner, N., Schmitt, C., Elbaum, M., Shorte, S. L., Danckaert, A. and Enninga, J. (2014). *Shigella* subverts the host recycling compartment to rupture its vacuole. *Cell Host Microbe* **16**, 517-530.

Miller, C. N., Smith, E. P., Cundiff, J. A., Knodler, L. A., Bailey Blackburn, J., Lupashin, V. and Celli, J. (2017). A *Brucella* type IV effector targets the COG tethering complex to remodel host secretory traffic and promote intracellular replication. *Cell Host Microbe*. **22**, 317-329.e7.

Myeni, S., Child, R., Ng, T. W., Kupko, J. J., III, Wehrly, T. D., Porcella, S. F., Knodler, L. A. and Celli, J. (2013). *Brucella* modulates secretory trafficking via multiple type IV secretion effector proteins. *PLoS Pathog.* **9**, e1003556.

Nixon-Abell, J., Obara, C. J., Weigel, A. V., Li, D., Legant, W. R., Xu, C. S., Pasolli, H. A., Harvey, K., Hess, H. F., Betzig, E. et al. (2016). Increased spatiotemporal resolution reveals highly dynamic dense tubular matrices in the peripheral ER. *Science* **354**, aaf3928.

Okiyoneda, T., Harada, K., Takeya, M., Yamahira, K., Wada, I., Shuto, T., Suico, M. A., Hashimoto, Y. and Kai, H. (2004). Delta F508 CFTR pool in the endoplasmic reticulum is increased by calnexin overexpression. *Mol. Biol. Cell* **15**, 563-574.

Pappas, G., Akritidis, N., Bosilkovski, M. and Tsianos, E. (2005). Brucellosis. *N. Engl. J. Med.* **352**, 2325-2336.

Pizarro-Cerda, J., Meresse, S., Parton, R. G., van der Goot, G., Sola-Landa, A., Lopez-Goni, I., Moreno, E. and Gorvel, J. P. (1998a). Brucella abortus transits through the autophagic pathway and replicates in the endoplasmic reticulum of nonprofessional phagocytes. *Infect. Immun.* **66**, 5711-5724.

Pizarro-Cerda, J., Moreno, E., Sanguedolce, V., Mege, J. L. and Gorvel, J. P. (1998b). Virulent *Brucella abortus* prevents lysosome fusion and is distributed within autophagosome-like compartments. *Infect. Immun.* **66**, 2387-2392.

Porte, F., Liautard, J. P. and Kohler, S. (1999). Early acidification of phagosomes containing *Brucella suis* is essential for intracellular survival in murine macrophages. *Infect. Immun.* **67**, 4041-4047.

Robinson, C. G. and Roy, C. R. (2006). Attachment and fusion of endoplasmic reticulum with vacuoles containing *Legionella pneumophila*. *Cell. Microbiol.* **8**, 793-805.

Schuck, S., Prinz, W. A., Thorn, K. S., Voss, C. and Walter, P. (2009). Membrane expansion alleviates endoplasmic reticulum stress independently of the unfolded protein response. *J. Cell Biol.* **187**, 525-536.

Smith, E. P., Miller, C. N., Child, R., Cundiff, J. A. and Celli, J. (2016). Postreplication roles of the *Brucella* VirB type IV secretion system uncovered via conditional expression of the VirB11 ATPase. *MBio* **7**, e01730-16.

Starr, T., Ng, T. W., Wehrly, T. D., Knodler, L. A. and Celli, J. (2008). *Brucella* intracellular replication requires trafficking through the late endosomal/lysosomal compartment. *Traffic* **9**, 678-694.

Starr, T., Child, R., Wehrly, T. D., Hansen, B., Hwang, S., López-Otin, C., Virgin, H. W. and Celli, J. (2012). Selective subversion of autophagy complexes facilitates completion of the *Brucella* intracellular cycle. *Cell Host Microbe* **11**, 33-45.

Taguchi, Y., Imaoka, K., Kataoka, M., Uda, A., Nakatsu, D., Horii-Okazaki, S., Kunishige, R., Kano, F. and Murata, M. (2015). Yip1A, a novel host factor for the activation of the IRE1 pathway of the unfolded protein response during *Brucella* infection. *PLoS Pathog.* **11**, e1004747.

Tilney, L. G., Harb, O. S., Connelly, P. S., Robinson, C. G. and Roy, C. R. (2001). How the parasitic bacterium *Legionella pneumophila* modifies its phagosome and transforms it into rough ER: implications for conversion of plasma membrane to the ER membrane. *J. Cell Sci.* **114**, 4637-4650.

Vergne, I., Chua, J., Singh, S. B. and Deretic, V. (2004). Cell biology of mycobacterium tuberculosis phagosome. *Annu. Rev. Cell Dev. Biol.* **20**, 367-394.

Journal of Cell Science (2018) 131, jcs210799. doi:10.1242/jcs.210799

Wang, X., Lin, P., Li, Y., Xiang, C., Yin, Y., Chen, Z., Du, Y., Zhou, D., Jin, Y. and Wang, A. (2016). *Brucella suis* vaccine strain 2 induces endoplasmic reticulum stress that affects intracellular replication in goat trophoblast cells in vitro. *Front. Cell Infect. Microbiol.* **6**, 19.

Zeuschner, D., Geerts, W. J. C., van Donselaar, E., Humbel, B. M., Slot, J. W., Koster, A. J. and Klumperman, J. (2006). Immuno-electron tomography of ER exit sites reveals the existence of free COPII-coated transport carriers. *Nat. Cell Biol.* **8**, 377-383.